




New empirical formula for nucleon-induced nonelastic cross sections based on two physical effects

Masahiro Nakano ¹, Yuji Yamaguchi ², and Yusuke Uozumi ³

¹New Medical Statistics Research Institute, 1245-11 Tateiwa, Iizuka, Fukuoka 820-0003, Japan

²J-PARC Center, Japan Atomic Energy Agency, 2-4 Shirakata, Tokai, Ibaraki 319-1195, Japan

³Department of Applied Quantum Physics and Nuclear Engineering, Kyushu University, 744 Motoooka, Nishi-ku, Fukuoka 819-0395, Japan



(Received 10 December 2020; revised 13 March 2021; accepted 24 March 2021; published 13 April 2021; corrected 28 April 2021)

A simple universal parametrization of nucleon-induced nonelastic cross sections is presented for a wide range of targets that is valid for the entire energy range from zero to a few gigaelectronvolts. We review several early studies by Letaw *et al.*, Pearlstein, Shen, Niita *et al.*, and Tripathi *et al.*, and our proposed approach differs completely from the formulas therein. The present formula is constructed based on recently discovered physical effects involving Coulomb repulsion and the discrete-level constraint and is based on the assumption that cross sections are continuous in both incident energies and targets. Our formula is given by a set of smooth functions of the mass number, which differs from the best formula to date by Tripathi *et al.* To compare our formula precisely with that by Tripathi *et al.*, we proposed the relative error index, which indicates the relative error between experimental data and predicted values. For the ¹²C, ²⁷Al, ⁵⁶Fe, ^{nat}Ag, ^{nat}Cd, ^{nat}Sn, ¹⁹⁷Au, and ²⁰⁸Pb targets used in this paper, the corresponding relative error indices show clearly that our formula is superior to that by Tripathi *et al.*

DOI: [10.1103/PhysRevC.103.044608](https://doi.org/10.1103/PhysRevC.103.044608)

I. INTRODUCTION

Defined as the total cross section minus the elastic-scattering cross section, the nucleon-induced nonelastic cross section (sometimes referred to as the total reaction cross section) includes all the reactions other than elastic scattering, such as particle emissions, inelastic scatterings, and absorptions. Nonelastic cross-section data below several gigaelectronvolts (GeV) are useful in many applications, such as designing nuclear plants, estimating medical treatment exposures, and material testing by cosmic rays. As these and related applications have become more sophisticated, a corresponding need has developed for detailed analysis tools in the form of both reliable theoretical models and accurate empirical formulas.

There are several dynamic models for describing nucleon-induced reactions, such as the intranuclear cascade (INC) model [1], quantum molecular dynamics [2], and antisymmetrized molecular dynamics [3]. Of these, INC models have been developed for better theoretical explanations of experimental data [4–8]. Recently, we have further developed the INC model to describe reaction data at lower energies [9–12], especially below 100 MeV including quantum effects [13–15]. As explained later, the results of those studies are used in the present paper.

Meanwhile, general empirical formulas to express nonelastic cross sections precisely are useful for phenomenological descriptions of data for any target and any incident energy, and there have been several such formulas for nucleon-induced nonelastic cross sections [16–21]. Those by Pearlstein [17], Shen [18], and Niita *et al.* [19] are old-fashioned formulas that

were not aimed at fitting cross sections below the Coulomb barrier, for example, below 10 MeV. However, since then there has been an accumulation of cross-section data from below the Coulomb barrier, thereby making that restriction obsolete. Therefore, in this paper we widen the range of incident energy to be from zero to a few GeV.

To construct our empirical formula, we use a completely different method from that used for the conventional formulas. It has been pointed out that quantum effects are important when applying the INC model at very low energies below the Coulomb barrier [13–15], and so we use that knowledge when creating our empirical formula.

The aim of this paper is to derive a new empirical formula for nucleon-induced nonelastic cross sections based on knowledge obtained from analyzing the INC model and in doing so show another way to construct empirical formulas. The derived empirical formula should be universal for any target mass and any incident energy and more precise than the conventional formulas. It is also important that the derived formula be expressed by differentiable functions, which is different from the formula by Tripathi *et al.* [21].

The proposed formula is aimed at being applicable to a wide range of targets from ¹²C to ²⁰⁸Pb and incident energies from zero to 2000 MeV, at least. The model parameters are adjusted to reproduce the nucleon-induced nonelastic cross sections of ¹²C, ²⁷Al, ⁵⁶Fe, and ²⁰⁸Pb targets, given that these nuclei were chosen as the targets of the INC model calculations in Refs. [13–15]. To test the parameters further, ^{nat}Ag, ^{nat}Cd, ^{nat}Sn, and ¹⁹⁷Au targets are added, although data above 100 MeV are scarce for these targets.

II. CONVENTIONAL EMPIRICAL FORMULAS

A. Formula by Letaw *et al.* and Pearlstein

For neutron-induced nonelastic cross sections, Letaw *et al.* [16] constructed a formula to reproduce the asymptotic value at high energies of a few GeV. The expression is very simple and comprises separate functions of the target mass number A and the incident energy E [16],

$$\begin{aligned}\sigma^n &= 45 A^{0.7} f^n(A) g^n(E), \\ f^n(A) &= 1 + 0.016 \sin[5.3 - 2.63 \ln(A)], \\ g^n(E) &= 1 - 0.62 \exp\left(-\frac{E}{200}\right) \sin(10.9E^{-0.28}).\end{aligned}\quad (1)$$

The cross sections and the incident energy are expressed in units of millibarns (mb) and megaelectronvolts (MeV), respectively. Although Eq. (1) was derived originally for proton-induced nonelastic cross sections, Pearlstein [17] claimed that at energies above the Coulomb barrier, the neutron-induced nonelastic cross section is about the same as the proton-induced one in which case Eq. (1) can also be used for neutron nonelastic cross sections above the Coulomb barrier.

B. Formula by Shen

For proton-induced nonelastic cross sections, based on Eq. (1) by Letaw *et al.* [16], Shen [18] generalized the formula

$$\begin{aligned}h_{\text{HE}}(A, E) &= 1 + \{[p\sigma_{\text{LE}}(A, E_c) + (1-p)1.1\sigma_{\text{HE}}(A, E_c)]\sigma_{\text{HE}}(A, E_c)^{-1} - 1\} \exp\{-\min[50, 0.1(E - E_c)]\}, \\ \sigma_{\text{LE}}(A, E) &= 1000\pi[0.14A^{1/3} + 0.122(A+1)A^{-1}\sqrt{14.1E^{-1}}]^2, \\ h_{\text{LE}}(A, E) &= 1 + \{[p\sigma_{\text{LE}}(A, E_c) + (1-p)1.1\sigma_{\text{HE}}(A, E_c)]\sigma_{\text{LE}}(A, E_c)^{-1} - 1\} \exp\{-\min[50, 0.1(E_c - E)]\}, \\ E_c &= 0.0575A + 12.31, \\ p &= \min(1, 0.684 + 1.327 \times 10^{-3}A),\end{aligned}\quad (4)$$

where $\min(a, b)$ indicates the smaller of a and b . The cross sections for proton injection are given by multiplying by the Coulomb factor f_{Coul} ,

$$\sigma^p = \sigma^n f_{\text{Coul}}. \quad (5)$$

The Coulomb factor f_{Coul} is unity above 200 MeV, and below 200 MeV it is written as

$$\begin{aligned}f_{\text{Coul}} &= f_{\text{C1}} f_{\text{C2}} q, \\ f_{\text{C1}} &= (1 + \exp\{\max[-50, (E_{\text{Coul}} - E)(3.816 + 0.1974Z)^{-1}]\})^{-1}, \\ f_{\text{C2}} &= (1 + \exp\{\max[-50, 0.5(E_{\text{Coul}} - E)]\})^{-1}, \\ q &= \begin{cases} 1 - \exp\{-\min[50, E^2(0.07246Z + 6.058)^{-2}]\} & (Z \geq 10), \\ 1 - \exp\{-\min(50, E^2/144)\} & (Z < 10), \end{cases} \\ E_{\text{Coul}} &= 1.44Z(8.2 + 0.68A^{1/3})^{-1},\end{aligned}\quad (6)$$

where Z is the atomic number and $\max(a, b)$ indicates the larger of a and b .

D. Formula by Tripathi *et al.*

Starting from the nonelastic cross section in the form given by Bradt and Peters [20], Tripathi *et al.* [21] developed a

by Pearlstein [17] to include the Coulomb effect by incorporating a multiplicative dumping function $h^p(A, E)$ due to the Coulomb effect,

$$\begin{aligned}\sigma^p &= 42.6 A^{0.701} f^p(A) g^p(E) h^p(A, E), \\ f^p(A) &= 1 + 0.0144 \sin[3.63 - 2.82 \ln(A)], \\ g^p(E) &= 1 - 0.67 \exp\left(-\frac{E}{150}\right) \sin(12E^{-0.289}), \\ h^p(A, E) &= 1/[1 + (0.018A^2 - 1.15A)E^{-2}].\end{aligned}\quad (2)$$

Here, the function $h^p(A, E)$ should be determined carefully because it has singular behavior. It gives negative values when $A < 64$ and $E^2 < \text{abs}(0.018A^2 - 1.15A)$.

C. Formula by Niita *et al.*

Following the formulas by Pearlstein [17] and Shen [18], Niita *et al.* [19] produced a generalized formula for low energies by incorporating multiplicative functions of the target mass and incident energy. The cross sections for neutron injection are given as

$$\sigma^n = \begin{cases} \sigma_{\text{HE}}(A, E) h_{\text{HE}}(A, E) & (E \geq E_c) \\ \sigma_{\text{LE}}(A, E) h_{\text{LE}}(A, E), & (E < E_c), \end{cases}$$

$$\sigma_{\text{HE}}(A, E) = 45A^{0.7} f^n(A) g^n(E), \quad (3)$$

where $f^n(A)$ and $g^n(E)$ are as expressed in Eq. (1). The functions h_{HE} and h_{LE} are given as follows:

formula that they claimed gave better agreement between calculated values and experimental data than could any earlier formula. However, the formula by Tripathi *et al.* [21] is very complicated, has many separate cases depending on mass A and charge Z of the target, and does not depend smoothly on target mass and energy. Because it is lengthy, the detailed expressions of the formula are given in the Appendix.

III. PROPOSED FORMULA BASED ON THE INC MODEL

Our strategy for formula development differs completely from those of the aforementioned pioneering studies. It is based on the physics of nucleon-induced reactions revealed by INC model analysis, which has been extended recently to reproduce cross sections at low energies below 100 MeV. It has been noted that two effects are important in this energy region, namely, that due to the discrete-level constraint (DLC) and that due to the Coulomb effect for proton injection, and it has been found that the DLC effect works for both proton- and neutron-induced reactions [15].

Here, we explain the two physical effects which were found in the extended INC model proposed recently [13–15]. The DLC effect is introduced to explain the limited freedom of excitation of the target nucleus induced by a nucleon with very low incident energy. When a very low-energy nucleon collides, the target cannot be excited unless a discrete excited state corresponding to the transition energy exists. Such a low-energy transition is then strongly restricted, which leads

to a sharp drop in the cross section at very low incident energy. This mechanism arises from quantum effects due to the few discrete levels at very low excitation energies. Thus, we refer to this effect as the DLC effect. For both neutron and proton injections, the DLC effect is confined to below ~ 50 MeV for light ^{12}C nuclei and to below 70 MeV for heavy ^{208}Pb nuclei. Importantly, the DLC effect is common for both neutron and proton injections, whereas the Coulomb effect appears only for proton injection. Herein, we follow these conclusions, and so each term of the proposed formula has physical meaning. If the two effects disappear completely, then a “bone structure” (as which we refer to) appears in the form of a gradually decreasing function of the incident energy, which comes from the nature of the bare two-body cross sections [22]. The target energy region of our formula is 0–2000 MeV as shown in this paper with experimental data, and moreover to 10 GeV if expanded without experimental data.

The neutron- and proton-induced nonelastic cross sections σ^n and σ^p , respectively, are given by

$$\begin{aligned}\sigma^n &= S_{\text{bone}}^n f_{\text{DLC}} f_{2G} + \sigma_{\text{reso}} f_{2G} + \sigma_{\text{asy}} \quad \text{for } n \text{ injection,} \\ \sigma^p &= S_{\text{bone}}^p f_{\text{DLC}} f_{\text{Coul}} f_{2G} + \sigma_{\text{reso}} f_{2G} + \sigma_{\text{asy}} \quad \text{for } p \text{ injection,}\end{aligned}\quad (7)$$

where S_{bone} represents the cross section of the bone structure, f_{DLC} is the factor indicating the DLC effect of the target, and σ_{reso} is the cross section originating from resonances,

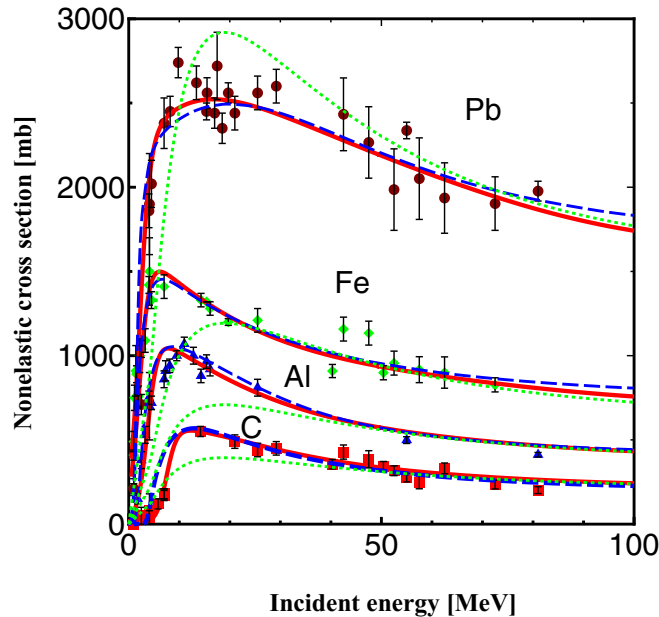


FIG. 1. Comparison between formula-predicted values by the three formulas and data of neutron-induced nonelastic cross sections for ^{12}C (red), ^{27}Al (blue), ^{56}Fe (green), and ^{208}Pb (brown) below 100 MeV. The solid red lines indicate our simulation results, the dashed blue lines indicate those by Tripathi *et al.* and the dotted green lines indicate those by Pearlstein. Note that for ^{12}C the experimental error bars are present but are covered by the plotting symbols.

such as $^{33}\Delta$ in the high-energy region above 1000 MeV. The factor f_{DLC} has the same form for both neutron and proton injections, and σ_{reso} is also assumed to be common for neutrons and protons, but f_{Coul} representing the Coulomb effect is for protons only. As shown later, the corrections f_{2G} and σ_{asy} are necessary when the formula is used for calculations with incident energy greater than 2000 MeV;

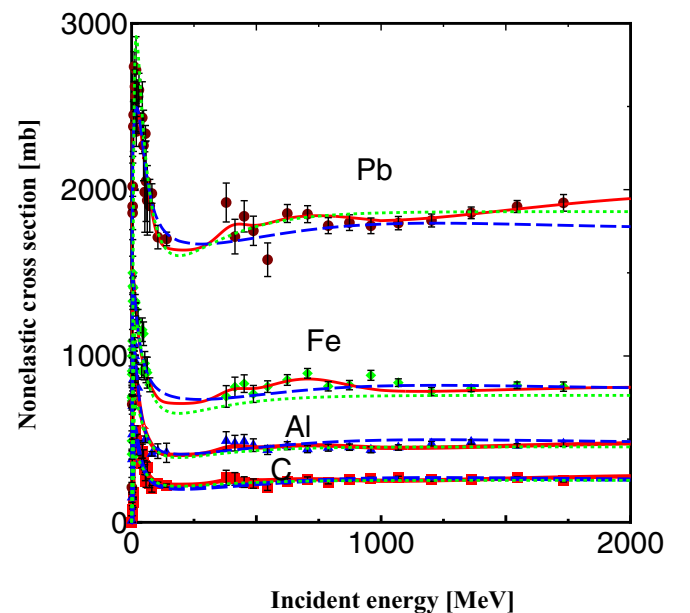


FIG. 2. As in Fig. 1 but with incident energies in the range of 0–2000 MeV for neutron-induced nonelastic cross sections.

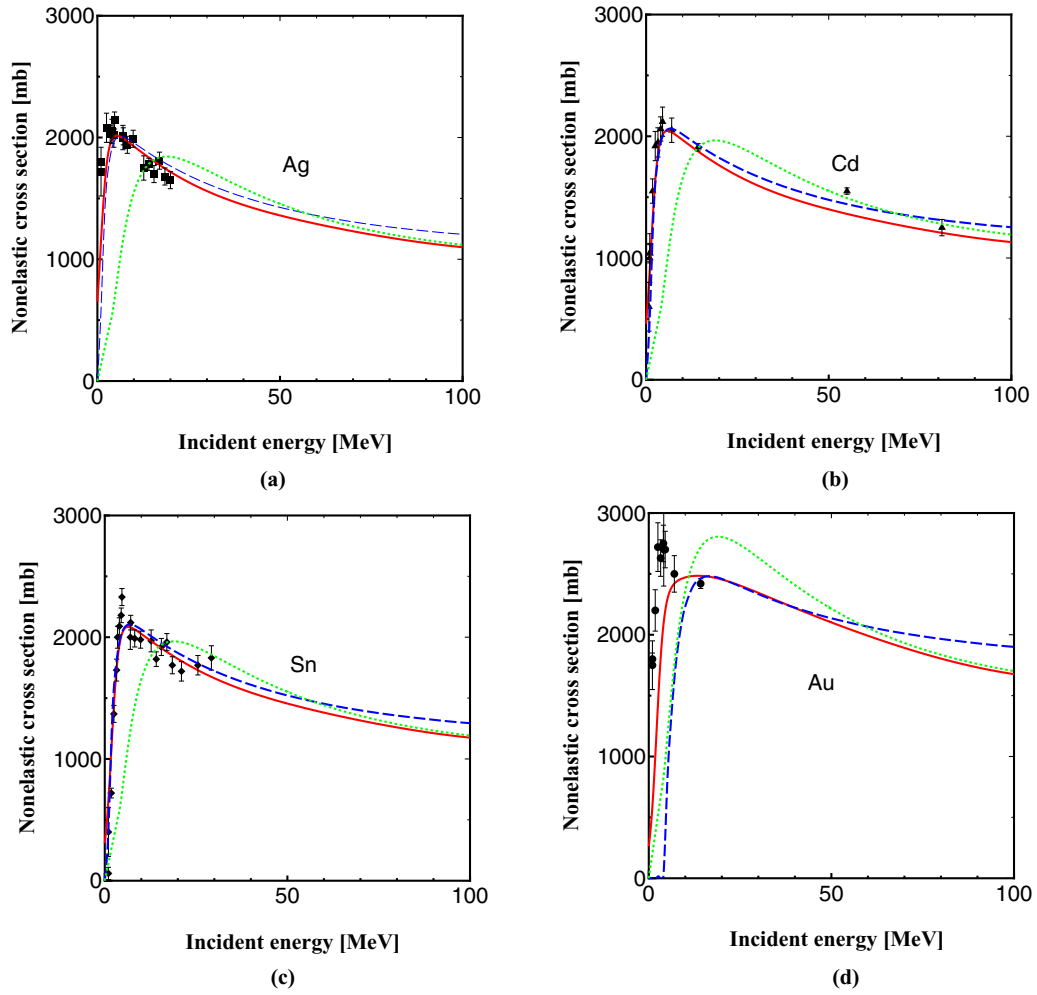


FIG. 3. Comparison between formula-predicted values and data for neutron-induced nonelastic cross sections for $^{\text{nat}}\text{Ag}$, $^{\text{nat}}\text{Cd}$, $^{\text{nat}}\text{Sn}$, and ^{197}Au below 100 MeV. The solid red lines indicate our simulation results, the dashed blue lines indicate those by Tripathi et al., and the dotted green lines indicate those by Pearlstein.

for calculations below 2000 MeV, results are the same as those as $f_{2G} = 1$ and $\sigma_{\text{asy}} = 0$.

The bone structure S_{bone}^n for neutron injection is given as follows:

$$S_{\text{bone}}^n = S_1 f_1 f_2,$$

$$S_1 = K_1 \left\{ 1 - 0.1 \exp \left[- \left(\frac{E - 250}{300} \right)^2 \right] \right\} \\ \times \left\{ 1 + 0.09 \exp \left[- \left(\frac{E - 60}{40} \right)^2 \right] \right\},$$

$$K_1 = 178(A + 30)^{0.385} \exp \left(- \frac{E^{1.07}}{30} \right) f_3 + C_1 + C_2,$$

$$C_1 = 10\pi(A^{1/3} + 0.17A^{0.42})^2,$$

$$C_2 = 6A^{0.5} \exp \left[- \left(\frac{E - 400}{80} \right)^2 \right] \\ + 6A^{0.5} \exp \left[- \left(\frac{E - 600}{400} \right)^2 \right],$$

$$f_1 = 1 + 0.1 \exp \left[- \left(\frac{A - 50}{20} \right)^2 \right],$$

$$f_2 = 1 + 0.07 \exp \left[- \left(\frac{A - 60}{20} \right)^2 \right] \exp \left[- \left(\frac{E - 700}{200} \right)^2 \right],$$

$$f_3 = \left\{ 1 + \frac{A^{1.2}}{400} \exp \left[- \left(\frac{E - 70}{50} \right)^2 \right] \right\} \\ \times \{ 1 - 0.06(A - 45) \exp[-0.01(A - 41)^2] \}, \quad (8)$$

where E (MeV) is the incident energy, A is the mass number, and the cross section is given in units of mb. The DLC factor f_{DLC} is given by

$$f_{\text{DLC}} = 1 / \{ 1 + \exp[-(E - E_1)] \} \\ \times 1 / \left\{ 1 + f_4 \exp \left[- \left(\frac{E - 10}{10} \right)^2 \right] \right\},$$

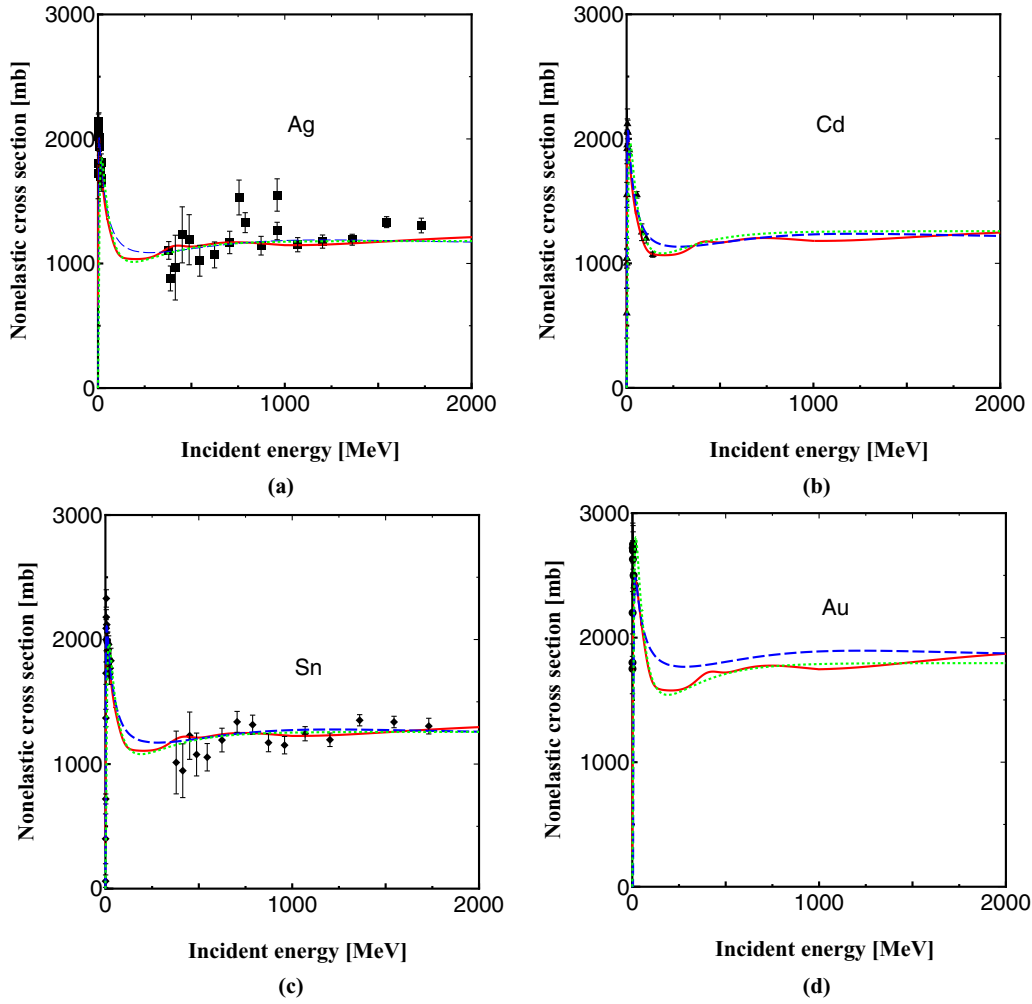


FIG. 4. As in Fig. 3 but with incident energies in the range of 0–2000 MeV for neutron-induced nonelastic cross sections.

$$\begin{aligned}
 E_1 &= \left(1.95 + \frac{180}{A^{1.4}}\right) \left[1 - 0.85 \exp\left(-\frac{(A-100)^2}{200}\right)\right] \\
 &\times \left[1 - 0.2 \exp\left(-\frac{(A-60)^2}{200}\right)\right], \\
 f_4 &= 0.28 \exp\left(-\frac{A-12}{10}\right) + 0.22 \exp\left(\frac{A-208}{50}\right).
 \end{aligned} \tag{9}$$

The resonance cross section σ_{reso} is given by

$$\begin{aligned}
 \sigma_{\text{reso}} &= \left(0.04 + \frac{A^{1.5}}{20000}\right) (E-1000) \\
 &\times 1/\{1 + 0.01 \exp[-(E-1000)]\}.
 \end{aligned} \tag{10}$$

The bone structure S_{bone}^p for proton injection is given as follows:

$$\begin{aligned}
 S_{\text{bone}}^p &= K_2 \exp\left(-\frac{E^{1.05}}{40}\right) + C_3 + C_4, \\
 K_2 &= (210+20A) \left\{1 - 0.12 / \left[1 + \exp\left(-\frac{A-160}{20}\right)\right]\right\} f_5,
 \end{aligned}$$

$$\begin{aligned}
 f_5 &= 1 - 0.05(A-45) \exp[-0.01(A-41)^2], \\
 C_3 &= 10\pi(A^{1/3} + 0.1A^{0.5})^2, \\
 C_4 &= 80 \left(\frac{A}{200}\right)^{0.2} \exp\left[-\left(\frac{E-1100}{800}\right)^2\right].
 \end{aligned} \tag{11}$$

The Coulomb factor f_{Coul} is given by

$$\begin{aligned}
 f_{\text{Coul}} &= f_6 f_7 f_8, \\
 f_6 &= 1/\{1 + \exp[-(E/V_M - 1.2)/0.75]\} \\
 f_7 &= 1/\{1 + \exp[-(E/V_M - 1.0)/0.1]\} \\
 f_8 &= 1/\{1 + \exp[-(E - 1.4V_M)/E_8]\}, \\
 E_8 &= 1.6(A+3)^{0.45} \left\{1 + 0.5 / \left[1 + \exp\left(-\frac{A-80}{10}\right)\right]\right\},
 \end{aligned} \tag{12}$$

where V_M is the maximum height of the Coulomb barrier for protons, which is the maximum of the sum of the Coulomb potential and nuclear potential; V_M and its radius R_M are given

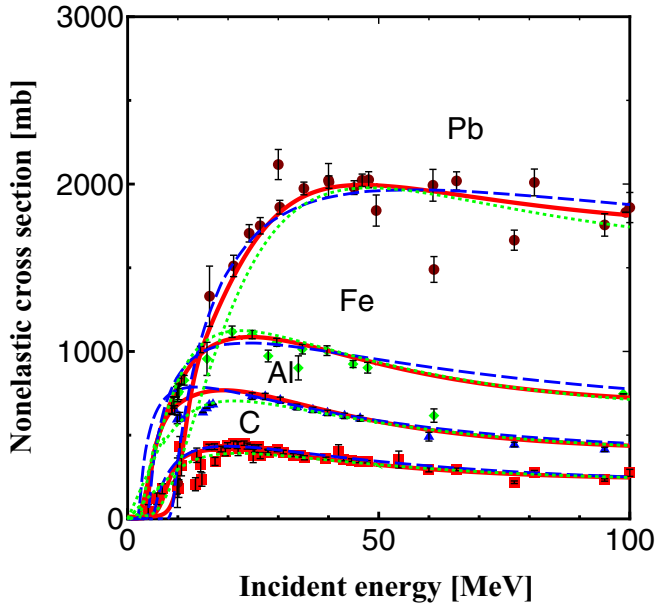


FIG. 5. Comparison between formula-predicted values and data for proton-induced nonelastic cross sections for ^{12}C (red), ^{27}Al (blue), ^{56}Fe (green), ^{208}Pb (brown) below 100 MeV. The solid red lines indicate our simulation results, the dashed blue lines indicate those by Tripathi et al., and the dotted green lines indicate those by Shen.

by the following overall fitting formula:

$$V_M = 0.2124 Z^{0.93} \left[1 - 0.72 \left(\frac{N-Z}{A} \right) \right],$$

$$R_M = 6.56 + 0.06Z \left[1 - 1.2 \left(\frac{N-Z}{A} \right) \right]. \quad (13)$$

These relations are derived from the INC model [15]. Finally, the corrections f_{2G} and σ_{asy} are used to reproduce the

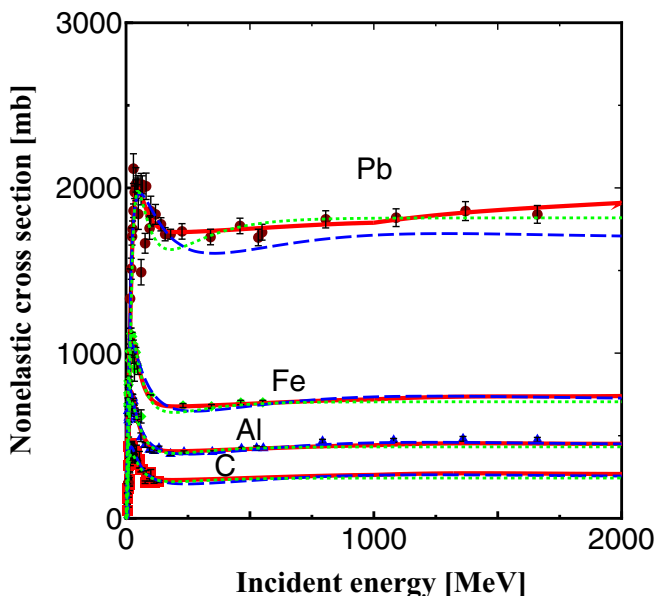


FIG. 6. As in Fig. 5 but with incident energies in the range of 0–2000 MeV for proton-induced nonelastic cross sections.

asymptotic cross section in the limit of very high energy up to 10 GeV and are given as

$$f_{2G} = 1/\{1 + \exp[(E - 2500)/500]\},$$

$$\sigma_{\text{asy}} = 45A^{0.7}/\{1 + \exp[-(E - 2500)/500]\}. \quad (14)$$

Because these factors have no effect on the nonelastic cross section below 2000 MeV, the corrections can be neglected for calculations below 2000 MeV by setting $f_{2G} = 1$ and $\sigma_{\text{asy}} = 0$.

IV. RESULTS AND DISCUSSION

We show the results separately in two regions of incident energy: The first is 0–100 MeV where our INC model [15] predictions agree excellently with experimental data [23], and the other is a wider range of 0–2000 MeV where some targets have few data points. The data points are insufficient in number and sometimes deviate considerably from the trend. We present our predicted results in Figs. 1–8, and for comparison we include those from other typical models, namely, Pearlstein [17] for neutron injection, Shen [18] for proton injection, and Tripathi et al. [21] for both cases. In the figures, the abnormal divergences given by Pearlstein and Shen near zero energy (which are explained later) are removed and smoothed for simplicity.

V. RELATIVE ERROR INDEX

The formulas by Pearlstein [17], Shen [18], and Niita et al. [19] have the merit of being given by simple equations. However, they have singular behavior at very low energies as shown in Fig. 9. The dotted lines by Shen have unphysical peaks and even negative values for $A < 63$ at energies below 5 MeV, the dashed lines by Niita et al. go to infinity because $\sigma_{\text{LE}}(A, E)$ contains the term $1/\sqrt{E}$ in Eq. (4), and the solid lines by Pearlstein have unnatural peaks at very low energy because of the sine function in $g^n(E)$ of Eq. (1). However, as noted earlier, these old-fashioned formulas were not aimed at reproducing the very low-energy region.

Only two formulas behave suitably and describe the experimental data satisfactorily in the entire incident-energy region, namely, our proposed formula and that by Tripathi et al. [21]. To compare these two formulas further, we require a quantity that indicates precisely the extent to which the experimental data are reproduced. For this purpose, we introduce the relative error (RE) index as

$$\text{RE} = \frac{1}{N} \sum \frac{\sqrt{(d_i - c_i)^2}}{(E_i^u + E_i^d)}, \quad (15)$$

where d_i is the value of experimental datum i , c_i is its formula-calculated value, E_i^u and E_i^d are the up and down error bar values for the datum i , and N is the total number of data in the summation. The RE index is akin to the χ^2 error but weighted by the error bars of the data. Thus, RE can be used as an indicator of model reproducibility. If $\text{RE} < 1$, then the calculated errors are small, being within the error bars of the measurements on average. In Table I, the values of the RE index for the proposed formula and that by Tripathi et al.

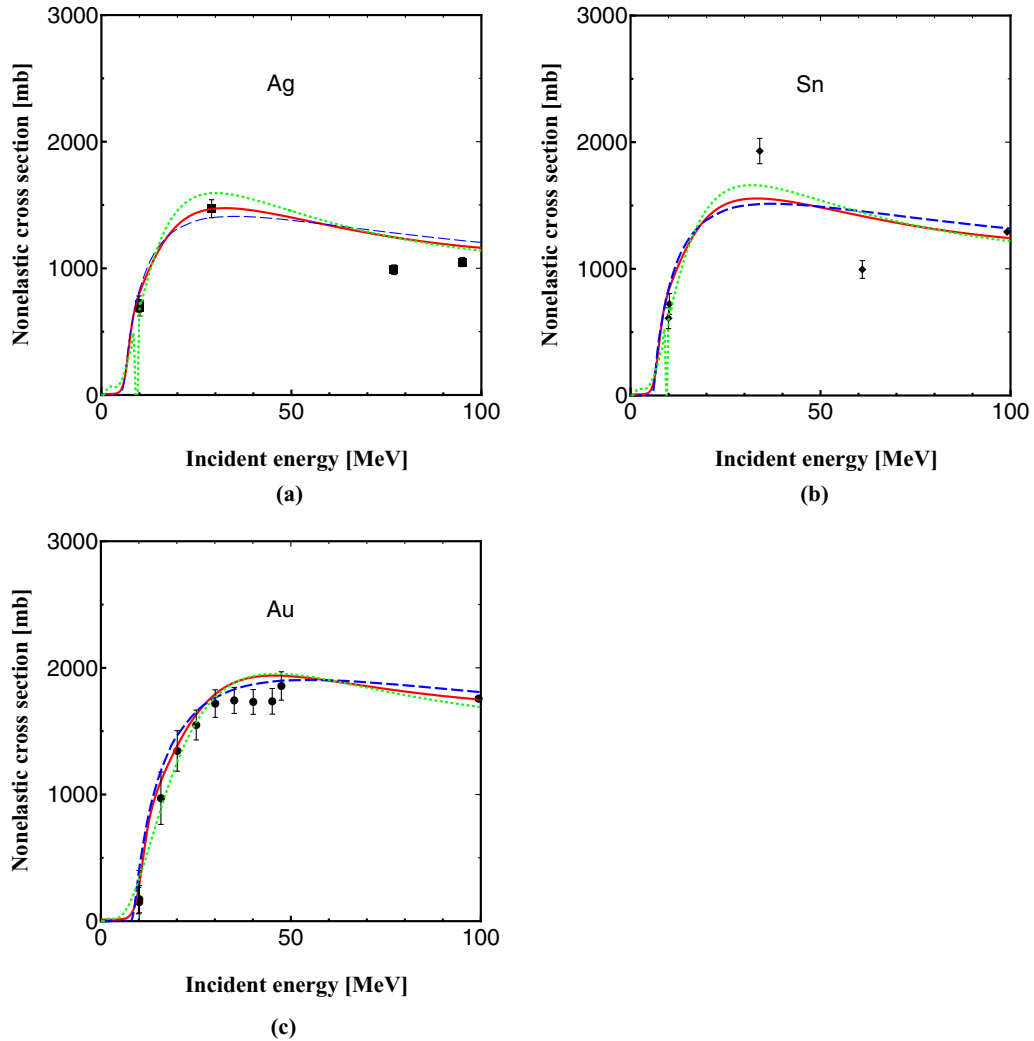


FIG. 7. Comparison between the predicted values by the three formulas and data of proton-induced nonelastic cross-sections for $^{\text{nat}}\text{Ag}$, $^{\text{nat}}\text{Sn}$, and ^{197}Au below 100 MeV. The solid red line indicates the result by our simulation, the dashed blue line indicates the result by Tripathi *et al.*, and the dotted green line by indicates the result Pearlstein.

[21] are given separately for neutron and proton injection. The RE index for the Cd target with proton injection is omitted because of the absence of data.

Table I shows clearly that the proposed formula is superior to that by Tripathi *et al.*, given that the values of the RE index for the former are smaller than those for the latter for all the targets. Note that the RE index with the proposed formula is less than one in every case except for $n + \text{Au}$. This indicates that the errors between the calculated values and the data are smaller than the experimental error bars on average. The reason why the RE index with the proposed formula is much bigger than one in the case of Au with neutron injection is that the cross-section data for Au at very low energies deviate largely from those for the other targets, for example, Pb. The prediction by the formula of Tripathi *et al.* is worse because the peak of the calculated cross section shifts to higher energy as shown in Fig. 3(d).

VI. TWO PHYSICAL EFFECTS

A. DLC effect from the proposed formula

We can separate out the DLC effect for any target by setting the factor f_{DLC} in Eq. (9) to one. The resulting cross sections without the DLC effect are compared with the full calculations with the DLC effect in Fig. 10. The DLC effect is shown by the difference between the solid and the dashed lines. In the neutron-induced cross section, the DLC effect is decisive for reproducing the experimental data at very low energies below 50 MeV.

B. Effect of Coulomb repulsion

The Coulomb effect can be recognized by setting $f_{\text{Coul}} = 1$ in Eq. (12). The dotted lines in Fig. 11 including the DLC effect alone show that the DLC effect makes the proton-induced

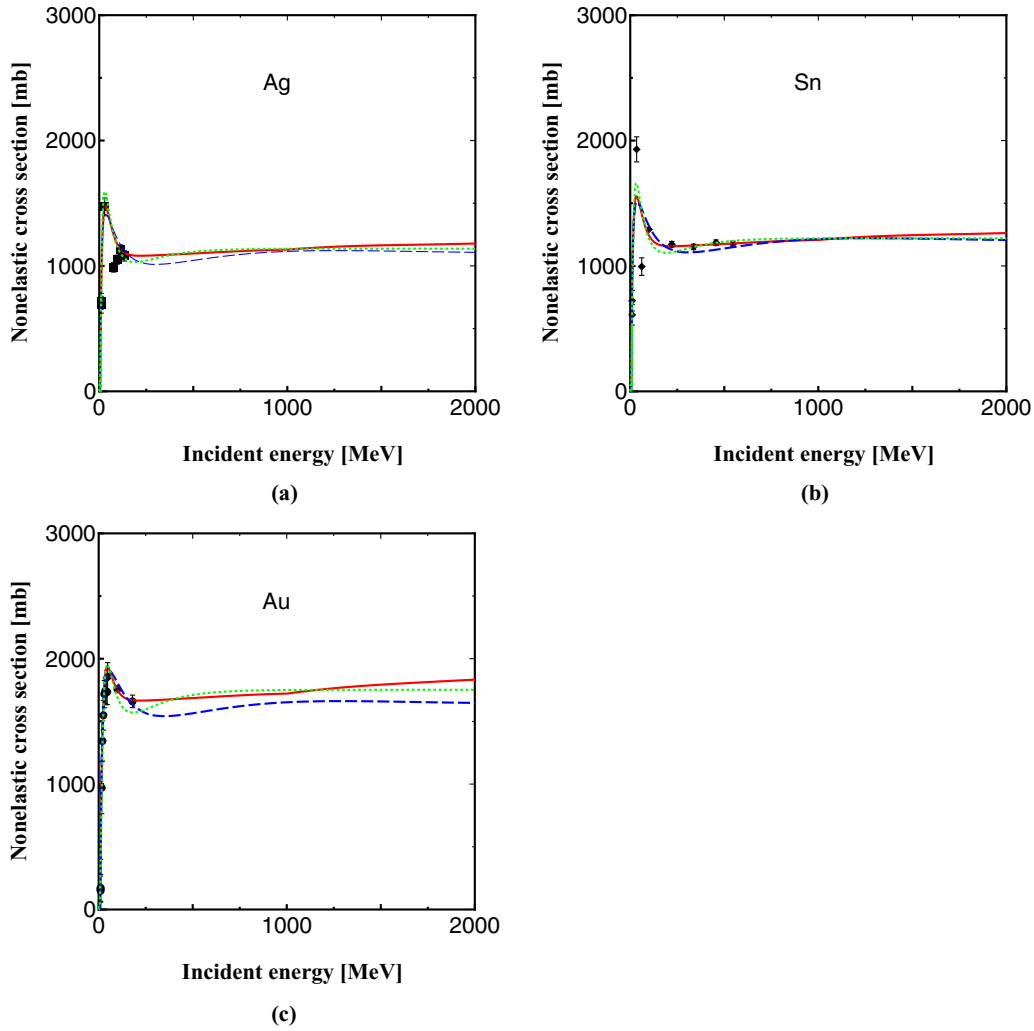


FIG. 8. As Fig. 7 but with incident energies in the range of 0–2000 MeV for proton-induced nonelastic cross sections.

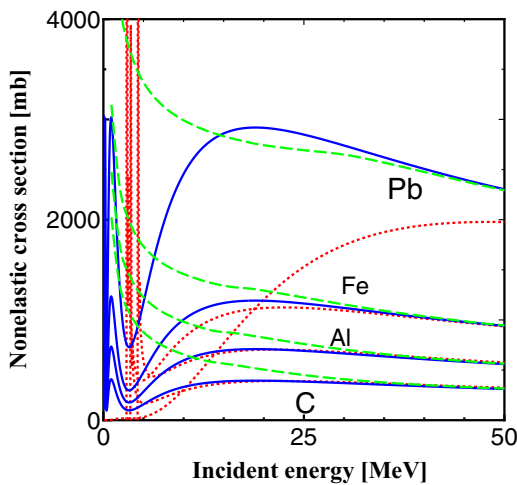


FIG. 9. Singular behavior of original formulas. The solid blue lines indicate the results using the formula by Pearlstein, the dashed green lines indicate those by Niita et al. for the n injection, and the dotted red lines indicate those by Shen for the p injection.

nonelastic cross sections similar to those of neutron injection. The difference between the dotted and the solid lines in Fig. 11 is due to the Coulomb effect, although the Coulomb effect overlaps partially with the DLC effect.

It is generally thought that proton-induced cross sections can be explained by the effect of Coulomb repulsion alone. All the earlier formulas are erroneous in constructing the

TABLE I. Comparison of values of the relative error index for the proposed formula and that of Tripathi et al. for neutron (n) and proton (p) injections.

n	C	Al	Fe	Pb	Ag	Cd	Sn	Au	Average
Tripathi et al.	0.79	0.81	0.72	0.77	0.68	1.29	0.84	6.89	1.60
Proposed	0.45	0.58	0.61	0.70	0.55	0.79	0.82	3.04	0.94
p	C	Al	Fe	Pb	Ag	Sn	Au	Average	
Tripathi et al.	0.79	0.77	0.98	0.79	1.48	1.34	0.5	0.95	
Proposed	0.77	0.53	0.53	0.53	0.99	0.88	0.42	0.67	

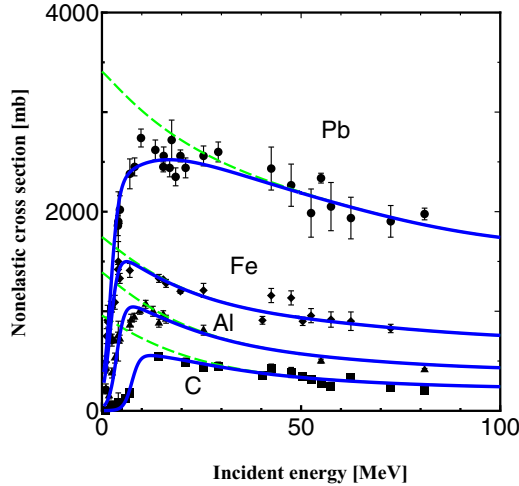


FIG. 10. Comparison between two calculations of neutron-induced nonelastic cross sections. The solid blue lines indicate the results of full calculations with the DLC effect, and the dashed green lines indicate those without the DLC effect.

proton-induced nonelastic cross section by multiplying the neutron-induced nonelastic cross section by the Coulomb dumping factor; this is a mistake because the DLC and the Coulomb effects coexist. Importantly, the two effects in Figs. 10 and 11 agree completely with those elucidated by our INC model calculations in Ref. [15].

VII. CONCLUSIONS

We have presented a simple universal parametrization of nucleon-induced nonelastic cross sections for any target and

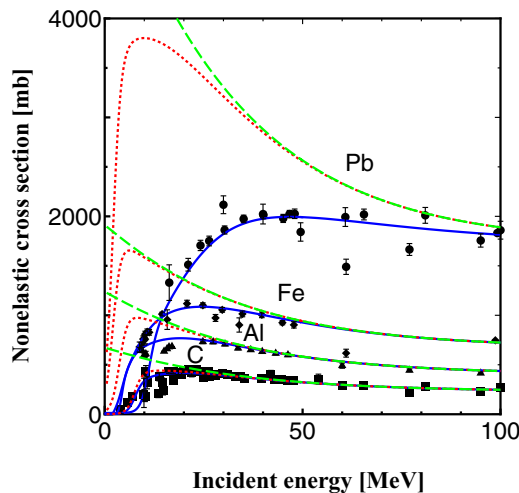


FIG. 11. Comparison between three calculations of proton-induced nonelastic cross sections. The solid blue lines indicate the results of full calculations with DLC and Coulomb effects, the dotted red lines show those without the Coulomb effect but with the DLC effect, and the dashed green lines show the bone structure resulting from neither DLC nor Coulomb effects. The difference between the dotted and the solid lines indicates the extent of the effect of Coulomb repulsion.

valid for the entire energy range from zero to a few giga-electronvolts. There are many ways to construct an empirical formula to describe experimental data, and in this paper we did so based on recently discovered physical effects. We began with the bone structures that are similar for neutron- and proton-induced nonelastic cross section, then we modified them by incorporating the physical effects of the DLC and Coulomb repulsion. The developed formula that includes these two physical effects can estimate their contributions separately for any target and any incident energy.

An important feature is that our formula is constructed based on the assumption that nonelastic cross sections change gradually with both incident energy and target, which is different from the formula by Tripathi et al. with its many separate cases. We note that the present formula cannot predict sharp changes if they exist, for example, sharp peaks, such as the shell effect in the very low-energy region. Instead, the formula should be considered as giving average values of nonelastic cross sections.

In this paper, we proposed the RE index that indicates the relative error between the experimental data and the predicted values. The quoted values of the RE index showed clearly that our formula is superior to that by Tripathi et al. for ^{12}C , ^{27}Al , ^{56}Fe , $^{\text{nat}}\text{Ag}$, $^{\text{nat}}\text{Cd}$, $^{\text{nat}}\text{Sn}$, ^{197}Au , and ^{208}Pb targets. Finally, we note that accumulating more complete experimental data in the future will allow a more precise formula to be constructed.

ACKNOWLEDGMENT

We thank members of the Uozumi Group at Kyushu University for their continuous support of this work.

APPENDIX

Tripathi et al. [21] started from the nonelastic cross section in the form given by Bradt and Peters [20],

$$\sigma_R = \pi r_0^2 (A_P^{1/3} + A_T^{1/3} + \delta)^2, \quad (\text{A1})$$

where r_0 is a unit radius, A_P and A_T are the projectile and target mass numbers, respectively, and δ is an energy-dependent parameter. This cross section originates from the geometrical cross section of the target nucleus plus projectile. Bradt and Peters aimed to describe nucleus-nucleus reaction

TABLE II. Values of k_B .

Target	k_B
$A_T > 56$	0.9
Ca	1.3
Si	1.4
Mg	1.8
$13 \leq A_T \leq 16$	$A_T/7$
$A_T = 12$	3.5
$A_T = 4$	27
$A_T < 4$	21
$A_T = 1$	21^2
Others	1

TABLE III. Values of T_1 for protons.

Target	T_1
Mg, Si, Ar, and Ca	40
$A_T > 45$ (except for above four)	$40 + A_T/3$
$A_T < 4$	55
Others	40

cross sections, which include nucleon-induced reaction cross sections as a typical case. The simple expression in Eq. (A1) deviates from experimental data in the low-energy region

below 100 MeV, although it gives a better description at higher energies. Therefore, Tripathi et al. [21] gave the reaction cross-section σ_R by modifying the Bradt-Peters form by incorporating complex dependences on the energy and target as follows:

$$\sigma_R = 10M\pi r_0^2 (A_p^{1/3} + A_T^{1/3} + \delta_E)^2 (1 - BE_{\text{cm}}^{-1}), \quad (\text{A2})$$

where $r_0 = 1.1$ fm and the unit of σ_R is mb. For protons, the normalization factor $M = 1$ in Eq. (A2), whereas for neutrons M is given as

$$M = \begin{cases} \{1 - 0.3 \exp[-\frac{E-1}{15}]\} \{1 - \exp[-(E-0.9)]\} & (A_T \geq 200), \\ 1 - M_1 \exp(-Ek^{-1}M_1^{-1}) & (A_T < 200). \end{cases}$$

$$M_1 = \max(1, 2.83 - 0.031A_T + 1.7 \times 10^{-4}A_T^2), \quad (\text{A3})$$

$$k = \begin{cases} 0.6 & (A_T < 12), \\ 1.6 & (A_T = 12), \\ 1 & (A_T > 12), \end{cases}$$

where E is the incident kinetic energy in the laboratory frame of reference. This is converted into the center-of-mass energy E_{cm} (MeV) in the collision frame of reference using the following equations:

$$E_{\text{cm}} = E_{\text{cm } p} + E_{\text{cm } T},$$

$$E_{\text{cm } p} = \gamma(E + 938)A_p - \beta\gamma P_{\text{lab}} - 938A_p,$$

$$E_{\text{cm } T} = 938A_T(\gamma - 1),$$

$$P_{\text{lab}} = A_p \sqrt{E^2 + 2 \times 938E},$$

$$\beta = \sqrt{1 - \gamma^{-2}},$$

$$\gamma = \{A_p(1 + E/938) + A_T\} \{A_p^2 + A_T^2 + 2A_p A_T(E/938 + 1)\}^{-1/2}. \quad (\text{A4})$$

The quantity B in Eq. (A2) is the energy-dependent Coulomb barrier and is given as

$$B = 1.44k_B Z_p Z_T R^{-1},$$

$$R = r_p + r_T + 1.2(A_p^{1/3} + A_T^{1/3})E_{\text{cm}}^{-1/3},$$

$$r_i = 1.29r_{\text{rms}, i} \quad (i = p, T),$$

$$r_{\text{rms}, i} = 0.84A_i^{1/3} + 0.55, \quad (\text{A5})$$

where Z_p and Z_T are the atomic numbers of the projectile and target, respectively. The factor k_B is listed in Table II.

The energy-dependent factor δ_E is given by

$$\delta_E = 1.85S - C_E + 0.16SE_{\text{cm}}^{-1/3} + 0.91(A_T - 2Z_T)Z_p A_T^{-1} A_p^{-1},$$

$$S = A_p^{1/3} A_T^{1/3} (A_p^{1/3} + A_T^{1/3})^{-1}, \quad (\text{A6})$$

$$C_E = D \{1 - \exp(-ET_1^{-1})\} - 0.292 \exp(-E/792) \cos(0.229E^{0.453}),$$

where T_1 is listed in Tables III and IV for protons and neutrons, respectively.

For protons, the coefficient D in Eq. (A6) is written as

$$D = \begin{cases} 1.7 & (\text{for } A_T < 4), \\ 2.05 - d/\{1 + \exp[0.1(E - 20)]\} & (\text{for Mg, Si, Ar}) \\ 2.05 - 1/\{1 + \exp[0.1(E - 40)]\} & (\text{for Ca}), \\ 2.05 - 0.05/\{1 + \exp[(250 - E)/75]\} & (\text{for others}) \end{cases} \quad (\text{A7})$$

where d is listed in Table V.

For neutrons, D is written

$$D = D_0 + \sum_{i=1}^5 c_i D_i$$

$$D_0 = 2 \times 0.134 457 \{0.5(\rho_{A_p} + \rho_{A_T})\}^{-1}$$

$$D_1 = Z_T (A_T - Z_T)^{-1}$$

$$D_2 = 1.5(A_T - 2Z_T)A_T^{-1}$$

$$D_3 = 2\{1 + \exp[0.05(E - 20)]\}^{-1}$$

$$D_4 = 0.25\{1 + \exp[-0.01(170 - E)]\}^{-1}$$

$$D_5 = \{1 + \exp[0.1(E - 20)]\}^{-1}$$

$$c_1 = \begin{cases} -1, & Z_T > 82, \\ 0, & \text{others,} \end{cases}$$

$$c_2 = \begin{cases} -1, & A_T < 60, \quad 140 < A_T < 200, \\ 0, & \text{others,} \end{cases}$$

$$c_3 = \begin{cases} -1, & Z_T \geq 82, \\ 0, & \text{others,} \end{cases}$$

$$c_4 = \begin{cases} 1, & A_T \leq 40, \\ 0, & \text{others,} \end{cases}$$

$$c_5 = \begin{cases} -1, & 10 \leq Z_T \leq 20, \\ 0, & \text{others,} \end{cases}$$

$$\rho_{A_i} = A_i \left(\frac{4}{3}\pi r_i^3\right)^{-1} \quad (i = p, T) \quad (\text{A8})$$

The formula by Tripathi et al. [21] is very complicated and has many separate cases for different masses A and charges Z .

Consequently, their predicted nonelastic cross sections at very low energies differ largely in different cases, even if dealing with two targets that are proximate elements, such as ^{197}Au and ^{208}Pb .

TABLE IV. Values of T_1 for neutrons.

Target	T_1
Si	35
Fe	30
$11 \leq A_T < 40$ (except for Si)	30
Others	40

TABLE V. Values of d .

Target	d
Mg	3
Si	1.75
Ar	2

- [1] R. Serber, *Phys. Rev.* **72**, 1114, (1947).
[2] J. Aichelin and H. Stocker, *Phys. Lett. B* **176**, 14 (1986).
[3] A. Ono, H. Horiuchi, T. Maruyama, and A. Ohnishi, *Prog. Theor. Phys.* **87**, 1185 (1992).
[4] J. Cugnon, *Nucl. Phys.* **A462**, 751 (1987).
[5] A. Boudard, J. Cugnon, S. Leray, and C. Volant, *Phys. Rev. C* **66**, 044615 (2002).
[6] T. E. Rodrigues, J. D. T. Arruda-Neto, A. Deppman, V. P. Likhachev, J. Mesa, C. Garcia, K. Shtejer, G. Silva, S. B. Duarte, and O. A. P. Tavares, *Phys. Rev. C* **69**, 064611 (2004).
[7] J. Cugnon, T. Aoust, A. Boudard, J. C. David, S. Pedoux, S. Leray, and Y. Yariy, *Adv. Space Res.* **40**, 1332 (2007).
[8] S. Pedoux and J. Cugnon, *Nucl. Phys.* **A866**, 16 (2011).
[9] Y. Uozumi, Y. Sawada, A. Mzhavia, S. Nogamine, H. Iwamoto, T. Kin, S. Hohara, G. Wakabayashi, and M. Nakano, *Phys. Rev. C* **84**, 064617 (2011).
[10] Y. Uozumi, T. Yamada, S. Nogamine, and M. Nakano, *Phys. Rev. C* **86**, 034610 (2012).
[11] Y. Uozumi, T. Yamada, and M. Nakano, *J. Nucl. Sci. Technol.* **52**, 263 (2015).
[12] Y. Uozumi, Y. Yamaguchi, G. Watanabe, Y. Fukuda, R. Imamura, M. J. Kobra, and M. Nakano, *Phys. Rev. C* **97**, 034630 (2018).
[13] M. Nakano and Y. Uozumi, *Phys. Rev. C* **100**, 034619 (2019).
[14] M. Nakano, Y. Yamaguchi, and Y. Uozumi, *Phys. Rev. C* **101**, 044616 (2020).
[15] M. Nakano, Y. Yamaguchi, and Y. Uozumi, *Phys. Rev. C* **102**, 024608 (2020).
[16] J. R. Letaw, R. Silberberg, and C. H. Tsao, *Astrophys. J., Suppl. Ser.* **51**, 271 (1983).
[17] S. Pearlstein, *Astrophys. J.* **346**, 1049 (1989).
[18] Q.-B. Shen, International Nuclear data committee INDC(CPR)-020 (1991), <https://www-nds.iaea.org/publications/indc/indc-cpr-0020/>.
[19] K. Niita, H. Takada, S.-I. Meigo, and Y. Ikeda, *Nucl. Instrum. Methods Phys. Res., Sect. B* **184**, 406 (2001).
[20] H. L. Bradt and B. Peters, *Phys. Rev.* **77**, 54 (1950).
[21] R. K. Tripathi, F. A. Cucinotta, and J. W. Wilson, NASA-Technical-Paper-3621, Langley Research Center, Virginia, 1997, https://www.researchgate.net/publication/2760249_NASA_Technical_Paper_3621.
[22] J. Cugnon, D. L. Hote, and J. Vandermeulen, *Nucl. Instrum. Methods Phys. Res., Sect. B* **111**, 215 (1996).
[23] Experimental Nuclear Reaction Data (EXFOR), <https://www.jcprg.org/exfor/> and references therein.

Correction: Equation (10) contained a minor error and has been fixed.